

**SYNTHESIS OF ORDERED MESOPOROUS SnO<sub>2</sub> USING SBA-15  
NANOCASTING TEMPLATE AND ITS PERFORMANCE AS A GAS  
SENSOR FOR HYDROGEN SULFIDE**

**By**

**RAM GHAUTAAM A/L P. RAMASAMY**

**UNIVERSITI SAINS MALAYSIA**

**2022**

**SYNTHESIS OF ORDERED MESOPOROUS SnO<sub>2</sub> USING SBA-15  
NANOCASTING TEMPLATE AND ITS PERFORMANCE AS A GAS  
SENSOR FOR HYDROGEN SULFIDE**

**By**

**RAM GHAUTAAM A/L P. RAMASAMY**

**Project proposal submitted in partial fulfilment of the requirement for degree of  
Bachelor of Chemical Engineering**

**2022**

## **ACKNOWLEDGEMENT**

Firstly, I would like to express my deepest gratitude towards my supervisor, Associate Professor Dr Zailani Abu Bakar who has guided me through completing this report with his knowledge and experience. Without his supervision and guidance, I would have not able to intricately write this report without any significant errors or mistakes.

I also would like to thank the School of Chemical Engineering, Universiti Sains Malaysia (USM) staff for their assistance and aid throughout this research study. Without their guidance and support, it would have been extremely hard for the collection of data and the analysis of parameters.

I also would like to thank my parents and friends for giving me the moral and financial support throughout my writing of this report.

Ram Ghautaam a/l P. Ramasamy

June 2022

## Table of Contents

<b>ACKNOWLEDGEMENT</b>	<b>I</b>
<b>TABLE OF CONTENTS</b>	<b>II</b>
<b>LIST OF TABLES</b>	<b>V</b>
<b>LIST OF SYMBOLS</b>	<b>VIII</b>
<b>LIST OF ABBREVIATIONS</b>	<b>IX</b>
<b>ABSTRAK</b>	<b>X</b>
<b>ABSTRACT</b>	<b>XI</b>
<b>CHAPTER 1</b>	<b>12</b>
<b>INTRODUCTION</b>	<b>12</b>
1.1 Air Pollutant Monitoring and Conventional Gas Sensors	12
1.2 Problem Statement	16
1.3 Research Objectives	17
<b>CHAPTER 2</b>	<b>18</b>
<b>LITERATURE REVIEW</b>	<b>18</b>
2.1 Properties of Metal Oxide Semiconductors	18
2.2 SnO <sub>2</sub> as a Gas Sensor	19
2.3 Synthesis of Ordered Mesoporous Metal Oxides	21
2.4 Synthesis of Ordered Mesoporous Silica	24
2.5 Optimum Temperature for the Performance of SnO <sub>2</sub> -Based Sensors	28
<b>CHAPTER 3</b>	<b>30</b>
<b>METHODOLOGY</b>	<b>30</b>
3.1 Research Flow	30

3.2.1	Materials	32
3.2.2	Equipment	33
3.3	Synthesis of SBA-15 Hard Template	34
3.4	Effect of Infiltration Method of Ordered Mesoporous SnO <sub>2</sub> synthesis	34
3.4.1	Conventional Evaporation Method (CEM)	34
3.4.2	Solid Liquid Method (SLM)	35
3.5	Effect of Infiltration Cycles on Ordered Mesoporous SnO <sub>2</sub> synthesis	35
3.6	Characterization of Ordered Mesoporous Silica and Ordered Mesoporous SnO <sub>2</sub>	35
3.6.1	X-ray Diffraction (XRD) Analysis	37
3.6.2	Brunauer-Emmet-Teller (BET) Analysis	37
3.6.3	SEM Analysis	38
3.7	MATLAB Coding for Sensitivity Analysis of Mesoporous SnO <sub>2</sub>	38
3.7.1	Model of Gas Diffusion	38
3.7.2	Effect of Operating Temperature on Sensitivity of Gas Sensor	40
3.7.3	Effect of Pore Size on Sensitivity of Gas Sensor	41
	<b>CHAPTER 4</b>	<b>43</b>
	<b>RESULTS AND DISCUSSION</b>	<b>43</b>
4.1	Characterization of Ordered Mesoporous Silica as a Hard Template	43
4.1.1	SEM Analysis of SBA-15 Morphology	43
4.1.2	XRD Analysis of SBA-15 Morphology	45
4.2	Characterization of Ordered Mesoporous SnO <sub>2</sub>	46
4.2.1	SEM Analysis of Different Types of Ordered Mesoporous SnO <sub>2</sub>	46

4.2.2	BET Analysis of Different Types of Ordered Mesoporous SnO <sub>2</sub>	48
4.3	XRD Analysis of Different Types of Ordered Mesoporous SnO <sub>2</sub>	51
4.4	Sensitivity Analysis	53
4.4.1	Effect of Pore Size on the Sensitivity of Gas Sensor	53
4.4.2	Effect of Operating Temperatures on the Sensitivity of Gas Sensor	56
<b>CHAPTER 5</b>		<b>60</b>
<b>CONCLUSION AND RECOMMENDATIONS</b>		<b>60</b>
5.1	Conclusion	60
5.2	Recommendations	61
<b>REFERENCE</b>		<b>62</b>
<b>CHAPTER 7</b>		<b>68</b>
<b>APPENDIX</b>		<b>68</b>
7.1	File: calledfunc.m	68
7.2	File: calledfunc1.m	68
7.3	File: k0_calculation.m	68
7.4	File: Diffusion_Constant.m	68
7.5	File: Poresize_Sensitivity.m	69
7.3	File:Operating_Temperature.m	70

## LIST OF TABLES

	<b>Title</b>	<b>Page</b>
<b>Table 3.1</b>	List of materials and chemicals	32
<b>Table 3.2</b>	List of equipment	33
<b>Table 3.3</b>	Sample types characterized via XRD analysis	36
<b>Table 3.4</b>	Sample types characterized via BET analysis	36
<b>Table 3.5</b>	Sample types characterized via SEM analysis	37
<b>Table 4.1</b>	BET specific area, adsorption average pore width the total pore volume of the SnO <sub>2</sub> replicas	50
<b>Table 4.2</b>	Crystallite sizes and d-spacings of SnO <sub>2</sub> replicas	52
<b>Table 4.3</b>	Experimental Values of Parameters	53
<b>Table 4.4</b>	Sensitivity of SnO <sub>2</sub> gas sensor with variation of pore size at 68.50 ppm and 333K	54
<b>Table 4.5</b>	Values of Parameters	56
<b>Table 4.6</b>	Sensitivity of SnO <sub>2</sub> gas sensor against variation of operating temperature at gas concentration of 100 ppm	57
<b>Table 4.7</b>	Sensitivity of SnO <sub>2</sub> gas sensor against variation of operating temperature at gas concentration of 200 ppm	57
<b>Table 4.8</b>	Sensitivity of SnO <sub>2</sub> gas sensor against variation of operating temperature at gas concentration of 300 ppm	58

## LIST OF FIGURES

Title	Page
<b>Figure 1.1</b> The working principle of electrochemical sensor in air and CO atmosphere	14
<b>Figure 2.1</b> Gas sensing mechanism of SnO <sub>2</sub> film	20
<b>Figure 2.2</b> Formation of mesoporous structures: (a) via cooperative self-assembly (b) via true liquid-crystal templating process	22
<b>Figure 2.3</b> Synthetic process of nanocasting	23
<b>Figure 2.4</b> XRD Analysis of MCM-41 mesostructures produced by conventional method (MCM-41/CM) and ultrasound method (MCM-41/UM)	25
<b>Figure 2.5</b> Illustration of the synthesis of SBA-15 mesostructure via hydrothermal treatment	27
<b>Figure 2.6</b> Gas-sensing response of the Cu-Zn doped SnO <sub>2</sub> replica at various operating temperatures to 50 ppm ethanol	29
<b>Figure 3.1</b> The Flow Diagram of the Methodology	31
<b>Figure 4.1</b> (a) SEM image of SBA-15 (20 kx) and (b) SEM image of SBA-15 (10kx)	43
<b>Figure 4.2</b> Wide-angle XRD pattern of SBA-15 silica synthesised under hydrothermal treatment of 80 °C	45
<b>Figure 4.3</b> (a) SEM image of SnO <sub>2</sub> -CEM (20 kx), (b) SEM image of SnO <sub>2</sub> -CEM (10kx) and (c) SEM image of SnO <sub>2</sub> -SLM (10kx)	46
<b>Figure 4.4</b> N <sub>2</sub> adsorption-desorption isotherms of (a) SnO <sub>2</sub> -1 cycle infiltration, (b) SnO <sub>2</sub> -2 cycle infiltration, (c) SnO <sub>2</sub> -3 cycle infiltration and (d) SnO <sub>2</sub> -SLM	48



<b>Figure 4.5</b> PSD curves of (a) SnO <sub>2</sub> -1 cycle infiltration, (b) SnO <sub>2</sub> -2 cycle infiltration, (c) SnO <sub>2</sub> -3 cycle infiltration and (d) SnO <sub>2</sub> -SLM	49
<b>Figure 4.6</b> Wide-angle XRD patterns of (a) SnO <sub>2</sub> -SLM (b) SnO <sub>2</sub> -1 cycle infiltration (c) SnO <sub>2</sub> -3 cycle infiltration and (d) SnO <sub>2</sub> -2 cycle infiltration	51
<b>Figure 4.7</b> Graph of Sensitivity of SnO <sub>2</sub> gas sensor against pore size simulated using MATLAB	54
<b>Figure 4.8</b> Graph of Sensitivity of SnO <sub>2</sub> gas sensor against operating temperatures simulated using MATLAB	58

## LIST OF SYMBOLS

<b>Symbol</b>	<b>Description</b>	<b>Unit</b>
<b>S</b>	Sensitivity of sensor	-
<b>R</b>	Gas constant	J/mol. K
<b>T</b>	Operating temperature of the sensor	K
<b>C<sub>s</sub></b>	Gas concentration outside the film	ppm
<b>L</b>	Thickness of the film	nm
<b><math>\alpha</math></b>	Sensitivity Coefficient	-
<b><math>\alpha_0</math></b>	Pre-exponential Constant	ppm <sup>-1</sup>
<b><math>k_0</math></b>	Pre-exponential Constant, obtained from A term in Equation	s <sup>-1</sup>
<b>E<sub>a</sub></b>	Apparent Activation Energy	J/mol
<b>E<sub>k</sub></b>	Activation Energy of the First Order Reaction	J/mol
<b>A</b>	Constant in equation of sensitivity of sensor,	nm <sup>-1</sup> K <sup>1/4</sup>
<b>r</b>	Pore radius	nm
<b>D<sub>c</sub></b>	Crystallite size	nm
<b>d<sub>110</sub></b>	d-spacing for (1 10) reflection index	-
<b>S<sub>BET</sub></b>	BET specific surface area	m <sup>2</sup> /g
<b>V<sub>T</sub></b>	Total pore volume	cm <sup>3</sup> /g
<b>kX</b>	1000 times (magnification)	-

## LIST OF ABBREVIATIONS

SBA-15	Saint Barbara Amorphous type material-15
BET	Brunnauer-Emmet-Teller
XRD	X-ray Diffraction
SEM	Scanning Electron Microscope
TEM	Transmission Electron Microscopy
IUPAC	The International Union of Pure and Applied Chemists
MCM-41	Mobil Composition Matter no.41
CEM	Conventional Evaporation Method
SLM	Solid Liquid Method
SBA-15-80	SBA-15 synthesised under hydrothermal aging temperature of 80 °C
SnO <sub>2</sub> -1 cycle infiltration	SnO <sub>2</sub> replicated from SBA-15 under 1 cycle of infiltration of CEM
SnO <sub>2</sub> -2 cycle infiltration	SnO <sub>2</sub> replicated from SBA-15 under 2 cycles of infiltration of CEM
SnO <sub>2</sub> -3 cycle infiltration	SnO <sub>2</sub> replicated from SBA-15 under 3 cycles of infiltration of CEM
SnO <sub>2</sub> -SLM	SnO <sub>2</sub> replicated from SBA-15 via SLM
TEOS	Tetraethyl orthosilicate

**SINTESIS SnO<sub>2</sub> BERLIANG MESO TERSUSUN MENGGUNAKAN TEMPANANO  
SBA-15 DAN PRESTASI SEBAGAI  
SENSOR GAS HIDROGEN SULFIDA**

**ABSTRAK**

Parameter yang diimplimentasi dalam sintesis SBA-15 berliang yang tersusun, sintesis replika SnO<sub>2</sub> berliang yang tersusun dan prestasi replika SnO<sub>2</sub> sebagai sensor gas hydrogen sulfida telah disiasat. SBA-15 berliang yang tersusun telah disintesis menggunakan kaedah tempa nano melalui kitaran infiltrasi berbeza dan kaedah infiltrasi yang berbeza. Kesahihan struktur berliang SBA-15 yang disintesis telah dibuktikan melalui kaedah penyifatan yang terdiri daripada analisis XRD, analisis BET dan analisis SEM. Sensitiviti replika SnO<sub>2</sub> yang berbeza telah disimulasi menggunakan MATLAB. Kod MATLAB telah disempurnakan dengan merujuk model matematikal yang dikemukakan dalam artikel yang spesifik dan telah dimodifikasi dengan merujuk artikel yang lain. Kesan saiz liang terhadap sensitiviti replika SnO<sub>2</sub> telah disiasat. Kesan suhu operasi dalam kepekatan gas yang berbeza terhadap sensitiviti replika SnO<sub>2</sub> juga telah disiasat. Daripada simulasi, saiz liang yang lebih besar menyumbang kepada sensitiviti yang lebih tinggi manakala prestasi optimum sensor gas dihubungkan dengan suhu 313 K.

**SYNTHESIS OF ORDERED MESOPOROUS SnO<sub>2</sub> USING SBA-15 NANOCASTING  
TEMPLATE AND ITS PERFORMANCE AS AGAS  
SENSOR FOR HYDROGEN SULFIDE**

**ABSTRACT**

The synthesis parameters of ordered mesoporous SBA-15 silica, ordered mesoporous SnO<sub>2</sub> replicas and the replicas performance as a gas sensor towards hydrogen sulfide gas has been investigated. Ordered mesoporous SBA-15 silica was first synthesised to produce a hard template for the nanocasting of SnO<sub>2</sub>. Ordered mesoporous silica was then produced using the SBA-15 hard template via nanocasting under different cycles of infiltration and different methods of infiltration. The validity of the mesostructure of the synthesised SBA-15 silica and ordered mesoporous SnO<sub>2</sub> replicas were proven by characterization methods involving XRD analysis, BET analysis and SEM analysis. The sensitivity of the different types of SnO<sub>2</sub> replicas were then simulated using MATLAB. The code was derived from the mathematical modelling of gas diffusion extracted from a specific literature and further modified by referring to other pieces of literature. The effect of pore sizes on the sensitivity of SnO<sub>2</sub> replicas towards hydrogen sulfide gas were investigated by using the pore radius data presented in the BET analysis. The effect of operating temperatures in different gas concentrations of hydrogen sulfide on the gas sensitivity of SnO<sub>2</sub> replicas were also investigated. The simulated results show that a larger pore radius corresponds to a higher gas sensitivity whereas the optimum performance of the SnO<sub>2</sub> gas sensor in different gas concentrations are attributed to a temperature of 313 K.

# CHAPTER 1

## INTRODUCTION

Chapter 1 introduces the overview of conventional gas sensors used for air pollutant monitoring and the inception of metal oxide semiconductors as new generation gas sensors. In general, chapter summarizes research background of gas sensors and how the introduction of metal oxide semiconductors improve the functionality of the gas sensors.

### 1.1 Air Pollutant Monitoring and Conventional Gas Sensors

One of the most serious environmental health problems of the modern times is air pollution. Air pollution can be defined as the introduction of chemicals, particulate matter or biological materials into the atmosphere that can lead to detrimental effects towards humans, other living organisms, and the environment (Soo, 2011). Air pollution sources include exhaust gases from automobiles, fossil fuel combustion, tobacco smoke, industrial amenities, and forest/agricultural fires (Dhall et al., 2021; Sun et al., 2012). Principal gases which result in outdoor air pollution are nitrogen oxides, carbon monoxide, sulphur oxides and greenhouse gases such as carbon dioxide and methane. Formaldehyde and volatile organic compounds (VOCs) are also identified as indoor air pollutants and their sources can be tracked down to applied construction materials and households. Air pollutants can be categorized as primary and secondary pollutants regardless of their form in either solid particles, liquid droplets, or gases. Primary pollutants are pollutants emitted directly from a process such as the exhaust gases of automobiles and ashes from a volcanic eruption. Secondary pollutants are not directly emitted from sources but instead are created from the reactions of primary pollutants. Ground level ozone is considered as a secondary pollutant (Soo, 2011).

Air pollutant monitoring has become of utmost importance to ensure the precise detection of toxic and deleterious air pollutants to curb air pollution's adverse effects towards the

environment and human health. The fundamental component of an air pollutant monitoring system are gas sensors. Gas sensors are vital in two primary areas of application, one being automated process control and another in the field of environmental protection (Weppner, 1987). Gas sensors are important devices to detect combustible, explosive, and toxic gases through the mechanism of initiating an alarm when the measured gas concentration exceeds the threshold value. Gas sensors are either portable or fixed devices. The four main parameters considered of designing a gas sensor are its sensitivity, selectivity, stability and speed while other minor but crucial parameters are recovery time, response time and power consumption. Gas sensors function through the primary principle of absorption and desorption of gas on the material surface, where the sensor records parameters such as resistance, temperature, acoustic wave, and capacitance through the interaction of the gas molecules with the surface atoms (Sarf, 2020). Conventional gas sensors include electrochemical sensors, gas chromatography, infrared spectroscopy, ultraviolet (UV) sensor with photoionization detector, chemiluminescent analysis and metal oxide semiconductors.

Electrochemical sensors are basically modified electrochemical cells for detecting gases in heavy gas dispersion systems where the strength of its signal is directly proportional to the partial pressure of gas in the atmosphere (Dhall et al., 2021). 3 types of solid electrochemical sensors, each possessing its own specific operating principle which include the direct measurement of the mobile species, indirect measurement of immobile components and analysis of other species by employing auxiliary solid phases (Weppner, 1987). Concentration of various analyte compounds in test samples are calculated by using electrochemical sensors. Electrochemical gas sensors are advantageous in the sense that they have a lower power consumption compared to other gas sensors, produce signals selective for the electrolyte's transferred component and the voltage related logarithmically covers a wider range of composition with precision (Weppner, 1987; Dhall et al., 2021). The lifespan of an

electrochemical sensor under standard conditions is estimated to be one year. However, electrochemical gas sensors have limitations, one being its selectivity provided for the transferred component. Although deviations from equilibria in the gas phase and across interfaces would be superimposed, misleading results may still be produced. The high sensitivity of electrochemical gas sensors is also limited by the decomposition of the solid separator and the exchange of small number of species between the phases at extremely low partial pressures (Weppner, 1987).

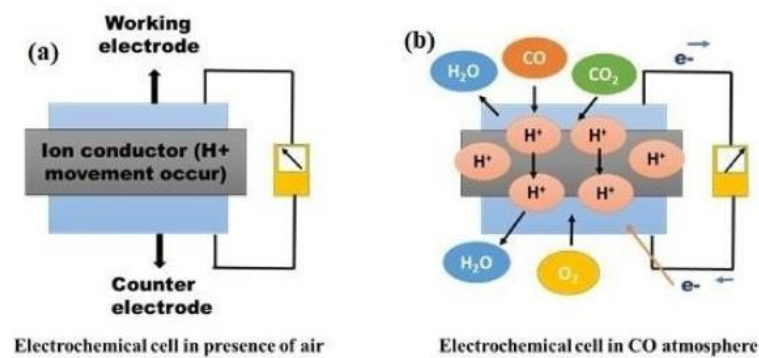


**Figure 1.1** The working principle of electrochemical sensor in air and CO atmosphere (Weppner, 1987)

Photoionization detector's (PID) working principle consists of the combined particles of ion mobility spectrometry, ionization energy discrimination and chemical filtering to verify the presence and measure the concentration of specific gases. For the detection of volatile organic compounds (VOCs), PID detectors are commonly preferred. The working mechanism of a PID is different from the flame ionization detector (FID) in the sense that the sample is not destroyed in the PID detector unlike in its counterpart, the FID. The operation of a PID begins with the introduction of a gas sample desired to be tested into the ionization chamber at one end of a drift tube. The gas molecules are ionized by the UV light that are controlled by multiple UV lamps or one multiple energy level UV lamp with different light band-width window zones and zone selector, where the intensity is varied based on the specific energy level needed for the



discrimination between potential constituents of the gas sample. The ionization chamber is separated a shutter grid from the drift tube. The opening of the shutter grid induces an electric field in the drift tube which attracts ions, travelling against the flow of the drift gas until it's collected by an electrode. A uniform electric field is sustained via thin mesh electrodes to ensure groups of ions travelling down the drift tube produce well-defined current pulses at the electrode collecting the ions (Chaulya and Prasad, 2016).

Metal oxide semiconductors (MOS) are being favoured by industries who are dependent on gas sensor technology to control and monitor combustion related emissions. Apart from detection of toxic/flammable/explosive gases, MOS are gaining popularity in air-quality monitoring and food processing due to their advantages over other types of gas sensing equipment. Gas detection systems such as infrared spectroscopy, gas chromatography and chemiluminescent analysis although having quick response times at the same time good detection limits, are still inferior MOS. MOS are more miniature and capable for selective *in situ* monitoring at wider temperature ranges (Saruhan et al., 2021). Moreover, metal oxides have an edge over other gas sensing equipment because they can detect low concentration of compounds in the air that possess weak gas-surface interactions, primarily minor chemisorption and physisorption (Kong et al., 2021). MOS gas sensors can be categorised into resistive and non-resistive types. MOS gas sensors consisting of surface and volume-controlled models are classified as resistive types. In surface-controlled models, the surface of the gas sensor makes close contact to the surface of the semiconductor energy band bending when the gas chemical adsorption on the surface of the components in the near-surface position creates a charge layer formation. Non-resistive types meanwhile consist of gas sensors with a diode rectifier function, field-effect transistor characteristics and capacitive functions. SnO<sub>2</sub> or more commonly known as tin dioxide is used in various traditional semiconductor gas sensors (Kong et al., 2021).

## 1.2 Problem Statement

The requirement of high working temperatures and poor selectivity of traditional SnO<sub>2</sub> gas sensors combined with the lack of adequate active sites limiting the adsorption of oxygen atoms to its surface, leads to poor performance (Kong et al., 2021). Ordered mesoporous SnO<sub>2</sub> as a gas sensor synthesised through the hard template method is indeed superior when compared to non-ordered mesoporous SnO<sub>2</sub> as well as mesoporous SnO<sub>2</sub> synthesized through the soft template method due to its larger surface area and improved thermal stability respectively.

However, different hard templates produce ordered mesoporous SnO<sub>2</sub> with different morphologies, grain/particle size and the crystal/electronic structures. These morphological and nanostructuring features affect the performance of the ordered SnO<sub>2</sub> as a gas sensor (Saruhan et.al, 2021). Higher porosity, crystallinity and surface area greatly improves the sensing mechanism of ordered mesoporous SnO<sub>2</sub>. One of the templates mentioned in the literature is the SBA-15 mesostructure, which will be utilized to produce the mesoporous SnO<sub>2</sub> focused on this work. The SBA-15 template also has uniform meso-ordered pore channels which functions to extensively regulate the particle size of the dopant and prevent the formation of debris from agglomeration (Tomer and Duhan, 2015).

The structure of the mesoporous metal oxide will be assessed using various methods such as the Brunnauer-Emmet-Teller (BET) surface area analysis method, the X-ray diffraction (XRD) analysis method and the transmission electron microscopy (TEM). The BET surface area analysis method is done through nitrogen desorption adsorption to calculate BET surface area, total pore volume and pore size (Li et al., 2007). The sensitivity and effectiveness of the mesoporous SnO<sub>2</sub> synthesized by SBA-15 template as a gas sensor is simulated using a MATLAB programme.

### **1.3 Research Objectives**

The objectives of this research:

- i. To synthesize and characterize SBA-15 hard template.
- ii. To synthesize and characterize ordered SnO<sub>2</sub> using SBA-15 hard template via nanocasting method
- iii. To study the performance of ordered SnO<sub>2</sub> sensing material at different operating temperatures and pore sizes

## CHAPTER 2

### LITERATURE REVIEW

In the previous chapter, the metal oxide gas sensor types were characterized, and a brief introduction of SnO<sub>2</sub> as a metal oxide semiconductor was given. The problem statement of this study was listed along with the objectives. In this chapter, the properties of metal oxide semiconductors are delved deeper along with a more detailed and comprehensive description of SnO<sub>2</sub> as a gas sensor. The description includes the working mechanism of SnO<sub>2</sub> as a gas sensor at the same time explaining the various nanostructures and morphologies of mesoporous SnO<sub>2</sub> based on literature. The different synthesis methods of mesoporous SnO<sub>2</sub> were compared with reference to articles containing study of mesoporous material synthesis including gas sensors. The morphology and synthesis of the mesoporous silica used as the hard template method is also described in this chapter.

#### 2.1 Properties of Metal Oxide Semiconductors

Due to their electronic charge transport properties, metal oxide semiconductors belong to a unique class of materials when compared to conventional covalent semiconductors such as silicon. Being valence compounds, metal oxide semiconductors have a high degree of ionic bonding. Metal oxide semiconductors can be classified into metal oxides with n-type conductivity and metal oxides with p-type conductivity. N-type metal oxide semiconductors predominantly have better electron transport due to their smaller electron effective mass whereas p-type metal oxide semiconductors have better hole transport due to their significantly smaller hole effective mass (He, 2020).

In<sub>2</sub>O<sub>3</sub>, ZnO and SnO<sub>2</sub> are typical metal oxide semiconductors with n-type conductivity. Cu<sub>2</sub>O, CuMO<sub>2</sub> and NiO metal oxide semiconductors can be identified as p-type semiconductors due to their more dispersive valence band maximum (VBM) relative to their n-type

counterparts (He, 2020). Metal oxide semiconductor devices are becoming promising elements for the future in the transitioning of modern electronics from being bulky, heavy and rigid to lightweight, flexible and compact. This is mainly due to the transparency, lightweight, biocompatibility and low-cost manufacturing of metal oxide semiconductors (Jo et al., 2020).

## **2.2 SnO<sub>2</sub> as a Gas Sensor**

SnO<sub>2</sub> or more widely known as tin dioxide is a semiconductor metal oxide manufactured as a gas sensor through morphological changes. SnO<sub>2</sub> is categorized as a post transition metal oxide which is more sensitive to the environment than pre-transition metal oxides which are relatively inert (Wang et al., 2010). SnO<sub>2</sub> is a n-type semiconductor oxide and has a large band gap of 3.6 eV (Das and Jayaraman, 2014). SnO<sub>2</sub> just like ZnO, WO<sub>3</sub> and In<sub>2</sub>O<sub>3</sub> are frequently used for the manufacturing of gas sensors with high detection speed, simplistic measurement procedures, small volume, and on-line monitoring. The functionalities of SnO<sub>2</sub> gas sensors are optimized through electrostatic spinning and hydrothermal methods (Li et al., 2020).

SnO<sub>2</sub>'s gas sensing mechanism is based on the variation of resistance caused by a manipulation of electron concentration resulting from gas adsorption and desorption. Oxygen in the air is first adsorbed by SnO<sub>2</sub> and dissociates into oxygen ions, leading to a change in the potential barrier between the SnO<sub>2</sub> grains and a change in resistance. The targeted gas under detection reacts with the adsorbed oxygen ions and the oxygen trapped electrons are released back to the conduction band of SnO<sub>2</sub>, decreasing the resistance of the gas sensor. The change of resistance is converted into an electric signal. The previous mechanism implies that the conductivity of SnO<sub>2</sub> depends on the density of oxygen ions adsorbed on the surface (Kong et al., 2021).

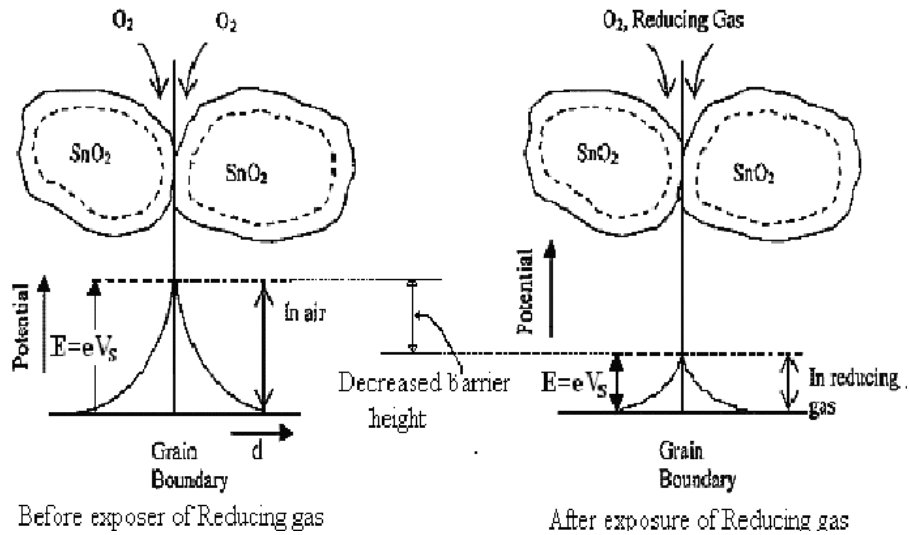
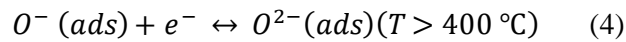
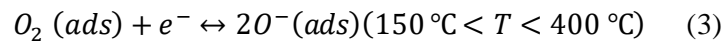
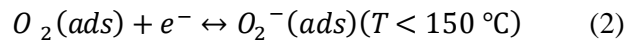
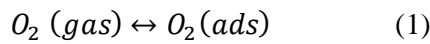


**Figure 2.1** Gas sensing mechanism of SnO<sub>2</sub> film (Manal Madhat Abdullah et al., 2012)

The adsorption process can also be explained by the following reactions:



Various nanostructures and morphologies cause different effects on the properties of the SnO<sub>2</sub> metal oxide gas sensors. The morphologies can range from 0-D to 3-D SnO<sub>2</sub> structures, each with their distinctive physical and chemical properties. For an example, with a 0-D morphology, SnO<sub>2</sub> structures have a high dispersitivity and ultra-small diameters, providing an enhanced performance of gas sensing by creating sufficient oxygen vacancies via a highly effective surface area. Freestanding 2-D structures on the other hand have an advantage over 3-D structures based on their optimization via the regulation of materials activity and surface polarization. Increase in surface area leading to a more effective mechanism in the adsorption and desorption of oxygen can also be achieved by ion doping,

which was clearly demonstrated by the Y-doped SnO<sub>2</sub> 3-D flower-shaped nanostructure containing many rough nanoflakes (Li et al., 2020).

SnO<sub>2</sub> structures are improved constantly by developing various synthesis methods to enhance their characteristics. Solution based methods are utilized to obtain nanostructures of metal oxides which have good control over shape, composition, and reproduction, promoting the usage of flexible parameters for mass production. The solution-based method can be further be categorized into the hydrothermal method and the precipitation method. Thermal conversion based on precursor solids is also another method for the development of SnO<sub>2</sub> nanostructures, involving the thermal dehydration of precursors in solid form with a relatively higher treatment temperature compared to the precipitation method. Electrochemical methods on the other hand are used to manufacture nano-porous metal oxides due to its simplicity and low operational temperatures, making commercial production feasible. The thermal oxidation method is used to create 1D morphology of metal oxide by heating the metal substrate to obtain the desired morphology (Yulianto et al., 2015).

### **2.3 Synthesis of Ordered Mesoporous Metal Oxides**

The synthesis of mesoporous metal oxides, including mesoporous SnO<sub>2</sub> are divided into three main methods, which is the conventional sol-gel method, the soft template method (utilization of self-assembled arrays of amphiphiles) and the hard template method (Cui et al., 2019; Wagner et al., 2006). Both types of templating methods, soft templating and hard templating involve the precursor and template material cooperating to build a mesoscopic ordered composite structure via some interaction force. By using the composite structure, SnO<sub>2</sub> can be transformed into 3-D interconnected and rigid skeletons through chemical synthesis. After chemical synthesis, the nanocasted template can be removed to obtain a mesoporous material on the nanometer scale (Cui et al., 2019).

The soft templating method utilizes the polymerization of surfactant molecules. In the soft template method, surfactants are used as a structure directing agent (SDA) as it possesses the crucial characteristic of the coexistence of a chemically bonded hydrophobic (non-polar) hydrocarbon ‘tail’ and a hydrophilic (polar) ‘head’ group in a molecule. Endotemplate methods (“soft-matter templating”) are the further classification of surfactant-assisted synthesis of mesoporous material including mesoporous metal oxides (Pal and Bhaumik, 2013). Through the soft templating route, inorganic precursors arrange themselves in an ordered array around the self-assembly of SDA to form an inorganic-organic composite solid in the liquid medium. As a result, the synthesized materials are amorphous in phase and after calcination at an elevated temperature, the amorphous phase becomes semicrystalline or crystalline, leading to a distorted porous structure with a relatively lower specific surface area (Hoa et al., 2015). The mesoporous metal oxide is obtained when the organic template is successfully removed from the inorganic-organic hybrid. The soft-templating route has two different mechanisms, the cooperative self-assembly and the liquid crystal template (TLCT) mechanism (Pal and Bhaumik, 2013).

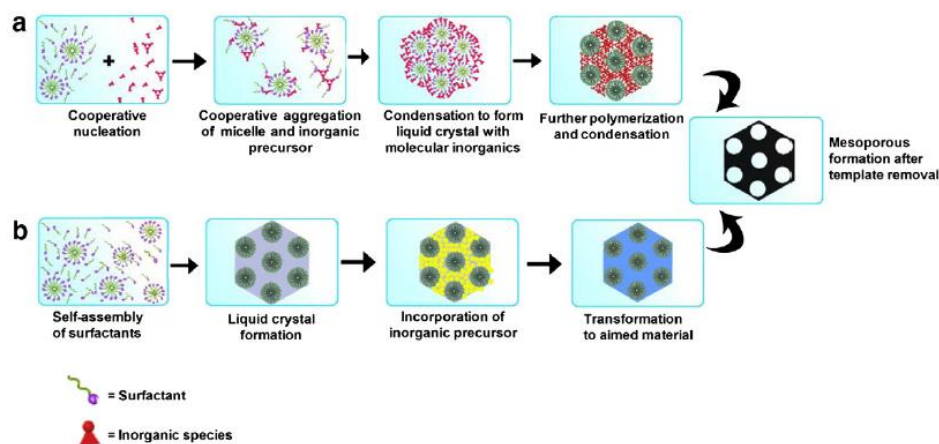


**Figure 2.2** Formation of mesoporous structures: (a) via cooperative self-assembly (b) via true liquid-crystal templating process (Pal and Bhaumik, 2013)



The soft template method of mesoporous metal oxides although have been researched for gas sensor applications, still have drawbacks such as disordered porous structures and low crystallinity (Hoa et al., 2015). Although the soft templating method is cost friendly and has a short-process time, it is inferior to the hard templating method due to the complex sol-gel chemistry and the fragility of the product towards experimental conditions. The complexity of controlling the oxide composition due to the interactions between surfactant and various precursors can affect the intake of metal ions, resulting in drastic change to the ordered mesoporous structure (Deng et al., 2016).

In the exotemplate or more commonly known as the hard template method, the production of mesoporous metal oxides is done via the usage of a solid material with a mesoscopic porous structure as a template (Cui et al., 2019). The first step of the hard template method involves the synthesis of the mesoporous templates. The usual templates used in synthesis of metal oxide gas sensors are mesoporous silica and carbon (Hoa et al., 2015). The second step is the infiltration of metal precursors. The third step is the elimination of the hard template to remove the pores (Zhang et al., 2019).

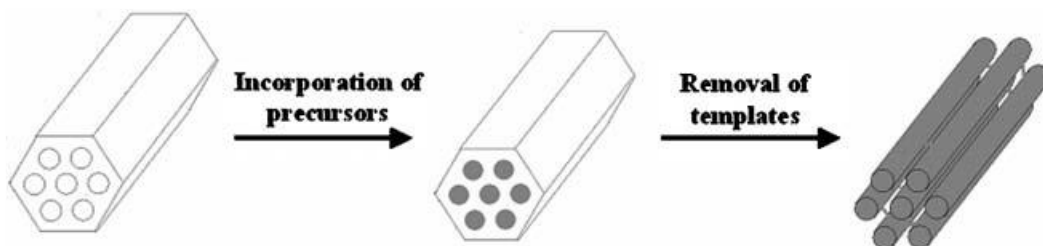


**Figure 2.3** Synthetic process of nanocasting (Yang and Zhao, 2005)

Through the hard template method, mesoporous semiconducting metal oxides such as ZnO, CeO<sub>2</sub>, MgO, Co<sub>3</sub>O<sub>4</sub> and Fe<sub>3</sub>O<sub>4</sub> have been successfully synthesized. Tungsten oxide can also be synthesized into a crystalline structure using mesoporous silica monoliths. Meanwhile, mesoporous cobalt oxide can be synthesized via hexagonal SBA-15 and three-dimensional cubic KIT-6 silica (Hoa et al., 2015).

Mesoporous silica is usually favoured as the hard template for the nanocasting of mesoporous metal oxides due to its enhanced thermal stability of the amorphous networks and strong grafting of organic functions (Pal and Bhaumik, 2013). The usage of mesoporous silica as a hard template is also advantageous because the diameters of the mesopores function as nanoreactors to ensure the replicated nanostructured arrays are also obtained in the same range. The mesostructures of the silicate templates also are the best cast to replicate highly ordered mesoporous metal oxides (Yang and Zhao, 2005). However, mesoporous silica itself is produced through the endotemplate method under hydrothermal treatment in basic or acidic conditions (Pal and Bhaumik, 2013).

The nanocasting method can be affected by the fluctuation of certain parameters which result in the failure of periodic replica mesostructures generating. These factors include the hydrogen bonding between the silicate walls and precursors, coordination bonding between hydroxy groups on the silica walls and the metal ions of the precursors and the coulombic interactions during the impregnation process of precursors (Yang and Zhao, 2005). Mesoporous silica itself can be classified into many types of templates. Some of these templates include KIT-6, SBA-15, SBA-16, and MCM-41 silica. SBA-15 has a two-dimensional channel-like structure whereas SBA-16 has a cage-like 3-D structure (Poonia et al., 2018).

## **2.4 Synthesis of Ordered Mesoporous Silica**

Widely used mesoporous silica can be classified into 3 categories which are MCM (Mobil Composition of Matters) from the M41S family, SBA (Santa Barbara Amorphous type materials) and the KIT-6 (Korea Advanced Institute of Science and Technology-6) (Deng et al., 2016; Sari Yilmaz et.al, 2013).

MCM-41 were one of the first hexagonal ordered mesoporous silica structures produced with pores larger than 2 nm. MCM-41 is synthesized via the addition of inorganic silica